Hindawi
Mathematical Problems in Engineering
Volume 2022, Article ID 1185792, 18 pages
https://doi.org/10.1155/2022/1185792

Research Article

Thermally Induced Bistable Functionally Graded Nanocomposite Plate

Yantao Zhu [1] **and Jixiao Tao** [2]

[1]*School of Civil Engineering and Architecture, Tibet Vocational Technical College, Lhasa 850000, China*
[2]*Department of Mechanics and Aerospace Engineering, Southern University of Science and Technology, Shenzhen 518055, China*

Correspondence should be addressed to Jixiao Tao; taojx@sustech.edu.cn

Received 18 October 2021; Accepted 23 December 2021; Published 17 January 2022

Academic Editor: Efstathios E. Theotokoglou

This paper explores the feasibility of using functionally graded carbon nanotube-reinforced composite (FG-CNTRC) in designing bistable plates. Single-walled carbon nanotubes (SWCNTs) in this nanocomposite are assumed to have a functionally graded distribution across the thickness direction following a power law. By varying the distribution type, volume fraction, and volume fraction exponent of SWCNTs, laminates with multiple thermal properties can be generated. A higher-order Rayleigh–Ritz model is presented to investigate the bistability and buckling behaviours of the proposed bistable plates. Their out-of-plane displacements and snap-through forces are predicted using this model. In the buckling analysis, transverse concentrated forces are applied to the panel corners to induce snap-through. To trace the load-displacement path during the loading process, the arc-length method is used to solve derived nonlinear equilibrium equations. The analytical results are compared using nonlinear finite element (FE) analysis for validation. A comprehensive parametric study is conducted to analyse the effects of curing temperature, distribution type, volume fractions, and volume fraction exponents of SWCNTs on the bistable behaviours of FG-CNTRC plates. It is found that, by varying these factors, bistable FG-CNTRC plates with multiple stable shapes and a wide range of snap-through forces can be generated. FG- CNTRC thus offers a rich design space for producing bistable plates.

1. Introduction

Bistable or multistable plates and shells have many potential applications in morphing structures and broadband energy harvesting and have attracted much research attention over the last few decades [1–7]. Commonly, bistable plates have two stable configurations and can transform from one equilibrium position to another in response to a small energy input. Because no external forces are needed to sustain the equilibrium configuration, they are good candidates for morphing skins in aerospace applications [8], wind-harvesting technology [9], and automobile construction [10]. In addition, bistable plates can be bonded with piezoelectric layers to create an energy harvester that can realise broadband energy harvesting [11, 12]. Internal structural bistability will make it possible to design small and portable piezoelectric energy harvesters in the future.

Thermally induced bistability is generally achieved by curing flat asymmetric laminates from high temperature to room temperature. During the cooling process, thermal residual stresses accumulate due to the mismatch of thermal expansion coefficients among cross-ply layers, which eventually lead to two stable shapes. Hyer [1] first explored this bistable behaviour in the early 1980s. At that time, laminates with an unsymmetric stacking sequence were avoided in manufacturing, due to the bending-stretching coupling effect. To qualify this effect, Dano and Hyer [3] developed an analytical model based on Kirchoff hypothesis with von Kármán geometric nonlinear strain in classical laminate plate theory (CLPT). Two stable shapes were predicted using Rayleigh–Ritz minimization of the total potential energy in conjunction with polynomial approximations of the mid-plane strains. Since then, increasing numbers of researchers have studied bistable structures. The literature in this area

now includes studies predicting stable shapes [13–15], calculating snap-through forces [4, 16, 17], and proposing new types of bistable structures [18–21]. However, traditional thermally induced bistable structures only have a few stable shapes, which limits their practical applications.

Variable stiffness multistable laminates have recently been proposed that offer a rich design space for bistable structures [22–25]. Mattioni et al. [22] investigated the equilibrium configurations of rectangular plates with partially unsymmetric stacking sequences subjected to a thermal field. Their results confirmed the possibility of obtaining systems that are both flexible and stiff, depending on the loading environment. Sousa et al. [23] modified the case of Mattioni et al. [22] and presented the concept of variable stiffness composite plates. In this study, curvilinear fibres were used in the unsymmetric regions of laminates to avoid stress concentrations at the interface. By comparing the snap-through behaviours of the variable stiffness laminate and the original straight fibre laminate, they found that the variable stiffness laminate needed a lower snap-through load, which may be beneficial for morphing applications. Haldar et al. [26] explored the multistable shapes of unsymmetric laminates with curvilinear fibres. Based on the semianalytical model developed in their work, a parametric study was conducted to analyse the effect of changing fibre orientation on the multistable shapes. They concluded that variable stiffness composite offers a rich design space for bistable configurations.

Functionally graded carbon nanotube-reinforced composite (FG-CNTRC) is very similar to variable stiffness composites, except that its material properties vary across the thickness direction. This type of composite was first proposed by Shen [27] who was inspired by the concept of functionally graded (FG) material. FG-CNTRC combines the merits of carbon nanotubes and polymers and is thus lightweight and possesses excellent mechanical properties [28, 29]. Recent mechanical analysis of FG-CNTRC has indicated its great potential for applications in structural vibration control and transportation engineering [30]. Given that the anisotropic thermal properties of composite are dominated by the fibre distribution types and directions, it is possible to design bistable laminates using functionally graded (FG) materials. However, to the best of the authors' knowledge, no publications to date have studied the bistablitity of FG-CNTRC plate.

In this paper, by combining CLPT with von Kármán geometric nonlinearity and following Rayleigh–Ritz minimization of the total potential energy, a higher-order analytical model is introduced to investigate the bistability of $[90/0]_T$ FG-CNTRC laminate. Because snap-through behaviour plays an important role in morphing applications, we adopt the arc-length method to determine the snap-through load. The analytical model is less accurate in predicting out-of-plane displacement near the edges and snap-through load; for this reason, a nonlinear finite element analysis is also conducted for validation, using the commercial FE software package ABAQUS. The primary goal of this paper is to investigate the influence of functionally graded distribution types, the volume fractions, and volume fraction exponents of single-walled carbon nanotubes (SWCNTs) on the stable shapes and snap-through forces of FG-CNTRC plates.

2. Effective Material Properties of FG-CNTRC Laminates

Cross-ply FG-CNTRC laminates with a length of L_x, width of L_y, and thickness of $2h$ are considered in this paper. As shown in Figure 1, the nanocomposite is made from a mixture of an isotropic matrix and SWCNTs, with graded distribution in the thickness direction. The effective mechanical constants of FG-CNTRC laminate, such as Young's modulus, shear modulus, and thermal expansion coefficients, can be predicted by the rule of mixture. The effective Young's modulus and shear modulus can be expressed as [31]

$$\begin{aligned} E_{11} &= \eta_1 V_{\mathrm{CN}} E_{11}^{\mathrm{CN}} + V_m^h E_h^m, \\ \frac{\eta_2}{E_{22}} &= \frac{V_{\mathrm{CN}}}{E_{22}^{\mathrm{CN}}} + \frac{V_m^h}{E_h^m}, \\ \frac{\eta_3}{G_{12}} &= \frac{V_{\mathrm{CN}}}{G_{12}^{\mathrm{CN}}} + \frac{V_m^h}{G_h^m}, \end{aligned} \tag{1}$$

where E_{11}^{CN}, E_{22}^{CN}, and G_{12}^{CN} are Young's modulus and shear modulus of SWCNTs, respectively, and E_h^m and G_h^m are the corresponding properties of the polymer matrix. The CNT efficiency parameter η_j $(j = 1, 2, 3)$ is used to account for the scale-dependent material properties, which can be determined by matching the effective properties of CNTRC simulated from molecular dynamics (MD) simulation with those from the rule of mixture. V_{CN} and V_m^h are the volume fractions of the carbon nanotubes and matrix and are related as follows:

$$V_{\mathrm{CN}} + V_m^h = 1. \tag{2}$$

Previous studies of CNTRC plate assumed a linear functionally graded distribution of SWCNTs. In this paper, however, we introduce an exponential distribution and consider the use of two types of FG-CNTRC (FGX and FGO) in designing bistable plates. The volume fraction V_{CN} satisfies the function list

$$V_{\mathrm{CN}} = \begin{cases} 2a\left|\dfrac{z}{h}\right|^n V_{\mathrm{CN}}^* \,(FGX - CNTRC), \\ 2a\left(1 - \left|\dfrac{z}{h}\right|\right)^n V_{\mathrm{CN}}^* \,(FGO - CNTRC), \end{cases} \tag{3}$$

in which

$$V_{\mathrm{CN}}^* = \frac{\omega_{\mathrm{CN}}}{\omega_{\mathrm{CN}} + (\rho_{\mathrm{CN}}/\rho_h^m) - (\rho_{\mathrm{CN}}/\rho_h^m)\omega_{\mathrm{CN}}}. \tag{4}$$

ω_{CN} is the mass fraction of the SWCNTs, and ρ_{CN} and ρ_h^m are the mass densities of the SWCNTs and matrix, respectively. To ensure that the FGX- and FGO-CNTRC plates have the same mass fraction of nanotube, the integral of V_{CN} through the thickness should satisfy

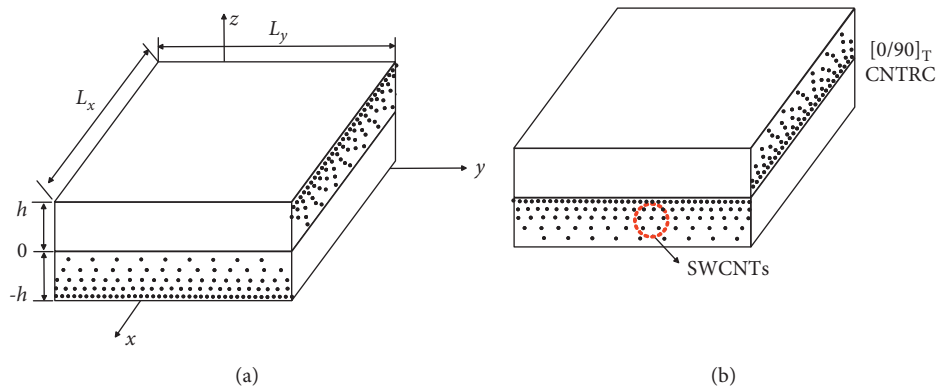

FIGURE 1: Functionally graded carbon nanotube-reinforced composite laminates with $[0/90]_T$ stacking sequence. (a) FGX-CNTRC laminate; (b) FGO-CNTRC laminate.

$$\int_{-h}^{h} V_{CN} dz = 2hV_{CN}^{*}. \tag{5}$$

The coefficient a in equation (3) can be determined by solving equation (5) for a given volume fraction exponent n.

The thermal expansion coefficients in the longitudinal and transverse directions can be expressed as

$$\begin{aligned} \alpha_{11} &= V_{CN}\alpha_{11}^{CN} + V_m^h \alpha_h^m, \\ \alpha_{22} &= \left(1+\nu_{12}^{CN}\right)V_{CN}\alpha_{22}^{CN} + \left(1+\nu_h^m\right)V_m^h\alpha_h^m - \nu_{12h}\alpha_{11}, \end{aligned} \tag{6}$$

where α_{11}^{CN}, α_{22}^{CN}, α_h^m, ν_{12}^{CN}, and ν_h^m are the thermal expansion coefficients and Poisson's ratio of the SWCNT and matrix. Poisson's ratio, ν_{12}, and mass density, ρ_{12}, of CNTRC can be expressed as

$$\begin{aligned} \nu_{12} &= V_{CN}^{*}\nu_{12}^{CN} + V_m^h\nu_h^m, \\ \rho_{12} &= V_{CN}\rho^{CN} + V_m^h\rho_h^m. \end{aligned} \tag{7}$$

It is assumed that the material properties of the SWCNTs and matrix are a function of temperature, so the effective material properties of FG-CNTRC are functions of temperature and position.

3. Analytical Model

3.1. Equilibrium Equation. The higher-order analytical model developed by Pirrera et al. [32] is extended in this paper. It is based on Classical Laminated Plate Theory (CLPT) with von Kármán nonlinear strains and the principle of minimum total potential energy.

Based on the Kirchhoff hypothesis in CLPT, the displacement field of the material point is defined by [33]

$$\begin{aligned} u(x,y,z) &= u_0(x,y) - z\frac{\partial w_0}{\partial x}, \\ v(x,y,z) &= v_0(x,y) - z\frac{\partial w_0}{\partial y}, \\ w(x,y,z) &= w_0(x,y), \end{aligned} \tag{8}$$

where u_0, v_0, and w_0 are the displacements of the mid-plane in the x, y, and z directions, respectively. For small strains and moderate rotations, the von Kármán nonlinear strains take the form

$$\begin{aligned} \varepsilon_{xx} &= \frac{\partial u}{\partial x} + \frac{1}{2}\left(\frac{\partial w}{\partial x}\right)^2, \\ \varepsilon_{xy} &= \frac{\partial v}{\partial y} + \frac{1}{2}\left(\frac{\partial w}{\partial y}\right)^2, \\ \varepsilon_{xy} &= \frac{1}{2}\left(\frac{\partial u}{\partial y} + \frac{\partial v}{\partial x} + \frac{\partial w}{\partial x}\frac{\partial w}{\partial y}\right). \end{aligned} \tag{9}$$

Substituting equations (8) into (9), the strain expressions reduce to

$$\begin{aligned} \begin{Bmatrix} \varepsilon_{xx} \\ \varepsilon_{yy} \\ \varepsilon_{xy} \end{Bmatrix} &= \begin{Bmatrix} \varepsilon_x^0 \\ \varepsilon_y^0 \\ \varepsilon_{xy}^0 \end{Bmatrix} + z\begin{Bmatrix} \kappa_{xx} \\ \kappa_{yy} \\ \kappa_{xy} \end{Bmatrix} \\ &= \begin{Bmatrix} \dfrac{\partial u_0}{\partial x} + \dfrac{1}{2}\left(\dfrac{\partial w_0}{\partial x}\right)^2 \\ \dfrac{\partial v_0}{\partial y} + \dfrac{1}{2}\left(\dfrac{\partial w_0}{\partial y}\right)^2 \\ \dfrac{\partial u_0}{\partial y} + \dfrac{\partial v_0}{\partial x} + \dfrac{\partial w_0}{\partial x}\dfrac{\partial w_0}{\partial y} \end{Bmatrix} + z\begin{Bmatrix} -\dfrac{\partial^2 w_0}{\partial x^2} \\ -\dfrac{\partial^2 w_0}{\partial y^2} \\ -2\dfrac{\partial^2 w_0}{\partial x\,\partial y} \end{Bmatrix}, \end{aligned} \tag{10}$$

where ε_x^0, ε_y^0, and ε_{xy}^0 are the membrane strains and κ_{xx}, κ_{yy}, and κ_{xy} are the flexural (bending) strains, known as curvature.

The linear constitutive relations for the k th orthotropic lamina, incorporating thermal effects, are expressed as

$$\begin{Bmatrix} \sigma_{xx} \\ \sigma_{yy} \\ \sigma_{xy} \end{Bmatrix}^{(k)} = \begin{bmatrix} \overline{Q}_{11} & \overline{Q}_{12} & \overline{Q}_{16} \\ \overline{Q}_{12} & \overline{Q}_{22} & \overline{Q}_{26} \\ \overline{Q}_{16} & \overline{Q}_{26} & \overline{Q}_{66} \end{bmatrix}^{(k)} \left(\begin{Bmatrix} \varepsilon_{xx} \\ \varepsilon_{yy} \\ \varepsilon_{xy} \end{Bmatrix} - \begin{Bmatrix} \alpha_{xx} \\ \alpha_{yy} \\ 2\alpha_{xy} \end{Bmatrix} \Delta T \right). \tag{11}$$

ΔT is the difference between curing temperature and room temperature, $\overline{Q}_{ij}^{(k)}$ is the transformed plane stress-reduced stiffness, and α_{xx}, α_{yy}, and α_{xy} are the transformed thermal coefficients of expansion. It should be noted that, for FG-CNTRC, $\overline{Q}_{ij}^{k}$ and α are functions of temperature and position z.

The force and moment resultants are then obtained by integrating the stresses through the laminates thickness:

$$\begin{Bmatrix} \mathbf{N} \\ \mathbf{M} \end{Bmatrix} = \begin{bmatrix} \mathbf{A} & \mathbf{B} \\ \mathbf{B} & \mathbf{D} \end{bmatrix} \begin{Bmatrix} \boldsymbol{\varepsilon}^0 \\ \boldsymbol{\kappa} \end{Bmatrix} - \begin{Bmatrix} \mathbf{N}^{\mathrm{T}} \\ \mathbf{M}^{\mathrm{T}} \end{Bmatrix}, \tag{12}$$

where $\mathbf{A}$, $\mathbf{B}$, and $\mathbf{D}$ are the extensional, coupling, and bending stiffness matrices and $\mathbf{N}^{\mathrm{T}}$ and $\mathbf{M}^{\mathrm{T}}$ are the thermal force resultants and thermal moment resultants, respectively. They are given by

$$(\mathrm{A}, \mathrm{B}, \mathrm{D}) = \sum_{k=1}^{N} \int_{z_k}^{z_{k+1}} Q_{ij}^{k} \left(1, z, z^2\right) \mathrm{d}z, \quad (i, j = 1, 2, 6). \tag{13}$$

$$\begin{aligned} \mathbf{N}^{\mathrm{T}} &= \sum_{k=1}^{N} \int_{z_k}^{z_{k+1}} \overline{Q}_{ij}^{k} \int_{T_c}^{T_r} \begin{Bmatrix} \alpha_{xx} \\ \alpha_{yy} \\ 2\alpha_{xy} \end{Bmatrix} \mathrm{d}T \, \mathrm{d}z, \\ \mathbf{M}^{\mathrm{T}} &= \sum_{k=1}^{N} \int_{z_k}^{z_{k+1}} \overline{Q}_{ij}^{k} \int_{T_c}^{T_r} \begin{Bmatrix} \alpha_{xx} \\ \alpha_{yy} \\ 2\alpha_{xy} \end{Bmatrix} \mathrm{d}T \, z \mathrm{d}z, \quad (i, j = 1, 2, 6), \end{aligned} \tag{14}$$

in which T_c and T_r are the curing and room temperature, respectively, and N is the number of plies.

According to the principle of minimum total potential energy, if no external work is considered, one can conclude that the first variation of the total potential energy is zero:

$$\int_{t_0}^{t} \delta \Pi \mathrm{d}t = 0$$

$$\Pi = \int_{-L_x/2}^{L_x/2} \int_{-L_y/2}^{L_y/2} \left(\frac{1}{2} \begin{Bmatrix} \boldsymbol{\varepsilon}^0 \\ \boldsymbol{\kappa} \end{Bmatrix}^{T} \begin{bmatrix} \mathbf{A} & \mathbf{B} \\ \mathbf{B} & \mathbf{D} \end{bmatrix} \begin{Bmatrix} \boldsymbol{\varepsilon}^0 \\ \boldsymbol{\kappa} \end{Bmatrix} - \begin{Bmatrix} \boldsymbol{\varepsilon}^0 \\ \boldsymbol{\kappa} \end{Bmatrix}^{T} \begin{Bmatrix} \mathbf{N}^{\mathrm{T}} \\ \mathbf{M}^{\mathrm{T}} \end{Bmatrix} \right) \mathrm{d}x \, \mathrm{d}y. \tag{15}$$

Stable configurations after the cooling-down process are determined by solving the preceding governing equations. Because an exact analytical solution of the midplane displacement field, u_0, v_0, and w_0 is very difficult to find, the Rayleigh–Ritz method can be used to obtain an approximate analytical solution. For laminates with free edge boundary conditions, the in-plane and out-of-plane displacement fields can be approximated by a complete polynomial basis truncated to order O_{pol}:

$$\begin{aligned} u_0(x, y) &= \sum_{m=0}^{O_{\mathrm{pol}}} \sum_{n=0}^{m} U_{n,m-n} x^n y^{m-n}, \\ v_0(x, y) &= \sum_{m=0}^{O_{\mathrm{pol}}} \sum_{n=0}^{m} V_{n,m-n} x^n y^{m-n}, \\ w_0(x, y) &= \sum_{m=0}^{O_{\mathrm{pol}}} \sum_{n=0}^{m} W_{n,m-n} x^n y^{m-n}. \end{aligned} \tag{16}$$

The displacement components in the preceding equations can be further reduced by imposing symmetries and boundary conditions. For the square $[90/0]_{\mathrm{T}}$ plates studied in this paper, the following conditions should be satisfied:

(1) $u_0(x, y)$ is odd in x and even in y

(2) $v_0(x, y)$ is even in x and odd in y

(3) $w_0(x, y)$ is even in x and y and vanishes at the origin

In the present study, order-5 displacement polynomials are used to predict the stable configurations and the snap-through forces, with the following forms:

$$\begin{aligned} u_0 &= U_{10}x + U_{02}y^2 + U_{12}xy^2 + U_{30}x^3 + U_{04}y^4 + U_{14}xy^4 \\ &\quad + U_{32}x^3y^2 + U_{50}x^5, \\ v_0 &= V_{01}y + V_{20}x^2 + V_{21}yx^2 + V_{03}y^3 + V_{40}x^4 + V_{41}x^4y \\ &\quad + V_{23}y^3x^2 + V_{05}y^5, \\ w_0 &= W_{20}x^2 + W_{02}y^2 + W_{22}x^2y^2 + W_{40}x^4 + W_{04}y^4. \end{aligned} \tag{17}$$

Substituting the approximate displacement expressions in equations (17) into (19), a set of nonlinear algebraic equations related to unknown coefficients $U_{n,m-n}$, $V_{n,m-n}$, and $W_{n,m-n}$ is obtained:

$$\partial \frac{\prod(\mathbf{c})}{\partial c_i} = \mathbf{f}(\mathbf{c}) = 0, \quad i = 1, 2, \ldots, 21, \tag{18}$$

where $\mathbf{c}$ represents the unknown vectors $\boldsymbol{U}$, $\boldsymbol{V}$, and $\boldsymbol{W}$ that uniquely define a specific stable configuration for a given curing temperature. Equation (20) is solved by the Newton–Raphson method and a stable solution is judged by its Jacobian matrix

$$J = \frac{\partial^2 \Pi}{\partial c_i \partial c_j}, \quad i, j = 1, 2, \ldots, 21. \tag{19}$$

An equilibrium configuration is stable if and only if the corresponding Jacobian matrix equation (19) is positive definite.

3.2. Snap-Through Load. Understanding the buckling behaviours of bistable FG-CNTRC laminates is important for practical applications. In the present research, the snap-through process is simulated by imposing point forces on each corner of the plate. Therefore, the virtual work done by external forces can be expressed as [16]

$$\delta W = F_x \delta u + F_y \delta v + F_z \delta w. \tag{20}$$

Because only transverse forces are applied, the virtual work in the x and y directions should be zero. Substituting the coordinates of the four corners into equation (17) and combining it with equation (20), we get

$$\begin{aligned}\delta W &= F_z\left[\delta w_0\left(\frac{-L_x}{2},\frac{-L_y}{2}\right) + \delta w_0\left(\frac{L_x}{2},\frac{-L_y}{2}\right) + \delta w_0\left(\frac{-L_x}{2},\frac{L_y}{2}\right) + \delta w_0\left(\frac{L_x}{2},\frac{L_y}{2}\right)\right] \\ &= F_z\left(\delta W_{20}L_x^2 + \delta W_{02}L_y^2 + \delta W_{22}\frac{L_x^4}{4} + \delta W_{40}\frac{L_x^2L_y^2}{4} + \delta W_{04}\frac{L_y^4}{4}\right).\end{aligned} \tag{21}$$

The principle of virtual displacements states that if the plate is in equilibrium, we must have

$$\int_{t_0}^{t} \delta(\Pi - W)\mathrm{d}t = 0. \tag{22}$$

If we combine equation (15) with equation (21) and substitute them into equation (22), the equilibrium equation governing the system becomes

$$\mathbf{K}(\mathbf{c}) - \mathbf{F} = 0. \tag{23}$$

It should be noted that because the geometric nonlinear terms are only related to the out-of-plane displacement, equation (23) is only a nonlinear function of the unknown vector $\boldsymbol{W}$. The force vector $\mathbf{F}$ thus has the form

$$\mathbf{F} = F_z\left\{L_x^2 \;\; L_y^2 \;\; \frac{L_x^4}{4} \;\; \frac{L_x^2L_y^2}{4} \;\; \frac{L_y^4}{4}\right\}^T. \tag{24}$$

To determine the snap-through force, we need to solve the nonlinear equation (23) iteratively by gradually increasing the transverse forces until a single solution is found [16]. This load-control method fails to follow the entire equilibrium path and may lead to difficulty in finding the solution near the bifurcation point. To investigate the whole buckling behaviour of bistable plates, this paper adopts the Riks arc-length method [34, 35] to trace the load-displacement diagram. In the arc-length method, both the load factor and the displacement increment are varied at each iteration to ensure the solution follows the equilibrium path until convergence is achieved [36]. To apply the arc-length method, the governing equation (23) can be modified as

$$\mathbf{K}(\mathbf{c}_0 + \Delta\mathbf{c}) - (\lambda_0 + \Delta\lambda)\mathbf{q} = \mathbf{0}, \tag{25}$$

$$\Delta\mathbf{c}^{\mathbf{T}}\Delta\mathbf{c} + \Delta\lambda^2\psi^2\mathbf{q}^{\mathbf{T}}\mathbf{q} = \Delta l^2, \tag{26}$$

where $\Delta\mathbf{c}$ is the vector of displacement increment and $\Delta\lambda$ is the incremental load factor, $\mathbf{c}_0$ and λ_0 are the corresponding solutions of the last equilibrium step, and Δl is the fixed radius of desired intersection that defines how far to search for the next equilibrium. First, the load factor can be set to zero to determine the initial equilibrium configuration. Once we obtain the stable shape after the cooling-down process, the corresponding solutions of U, V, and W are used as starting values for equations (25)-(27) to initiate the arc-length method. The loading process is terminated when the corner out-of-plane displacement reaches another equilibrium point. Based on the simulated load-displacement diagram, the snap-through forces can be easily determined. All of the simulation processes in the analytical model described here are realised using our developed MATLAB code.

4. Finite Element Simulations

The analytical approach outlined in the previous section can achieve fast simulations and hence is suitable for parametric studies. However, as has been reported by many researchers [4, 16], its accuracy drops when predicting out-of-plane displacement near edges and calculating snap-through forces. Although increasing the order of displacement polynomials equation (18) can improve accuracy, problems in finding stable solutions of the derived nonlinear algebraic equations may occur at the same time. For validation, we perform a nonlinear FE analysis using the commercial FE software package ABAQUS. It has been shown that FE simulations can achieve good agreement with experimental results for both the cooling-down and snap-through process [37]. It should be noted that, in analysing functionally graded material, it is not possible to assign continuously variable material properties across the thickness direction in ABAQUS. Instead, we can specify the equivalent section properties directly for conventional shells in the "property module." This approach requires users to input the section stiffness properties and the thermal stresses [38].

In ABAQUS, the shell section response is defined by

$$\{\mathbf{N}\} = Y\left(\theta, f_\beta\right)[\mathbf{D}]\colon \{\mathbf{E}\} - \left\{\mathbf{N}^{\mathrm{th}}\right\}. \tag{27}$$

$\{\mathbf{N}\}$ is the forces and moments on the shell section (membrane forces per unit length, bending moments per unit length);

$\{\mathbf{E}\}$ is the generalised section strains in the shell (reference surface strains and curvatures); the order of the components is

$$\begin{aligned}\{\mathbf{N}\} &= \{N_{11} \;\; N_{22} \;\; N_{12} \;\; M_{11} \;\; M_{22} \;\; M_{12}\}^T, \\ \{\mathbf{E}\} &= \{\varepsilon_{11} \;\; \varepsilon_{22} \;\; \gamma_{12} \;\; \kappa_{11} \;\; \kappa_{22} \;\; \kappa_{12}\}^T.\end{aligned} \tag{28}$$

$[\mathbf{D}]$ is the section stiffness matrix

$$[\mathbf{D}] = \begin{bmatrix} \mathbf{A} & \mathbf{B} \\ \mathbf{B} & \mathbf{D} \end{bmatrix}. \quad (29)$$

$Y(\theta, f_\beta)$ is a scaling modulus, which can be used to introduce the temperature (θ) and field-variable (f_β) dependence of the cross section stiffness.

And $\{\mathbf{N}^{\text{th}}\}$ is the section forces and moments (per unit length) caused by thermal stresses.

$$\{\mathbf{N}^{\text{th}}\} = \left(\alpha\left(\theta, f_\beta\right)\left(\theta - \theta^0\right) - \alpha\left(\theta^I, f_\beta^I\right)\left(\theta^I - \theta^0\right)\right)\{F\}. \quad (30)$$

For FG-CNTRC laminates with different functionally graded distributions and volume fractions of SWCNTs, we can input the corresponding **ABD** matrices and thermal stresses to implement FE analysis. Details of the nonlinear FE analysis are given in the next subsection.

4.1. Analysis of the Cooling-Down Process. With a square FG-CNTRC plate, initial geometrical imperfections or small external forces should be imposed to make the plate converge to one of the stable shapes [26, 32, 37]. Because the introduced geometrical imperfections will influence the snap-through forces, applying external force is the preferred method. The plate is modelled using a 1600 4-node, quadrilateral shell element (S4R) with a total of 1681 nodes. By fixing the middle point of the panel, the cooling-down process in ABAQUS is achieved by using two "static, general" steps with "geometric nonlinearity." In the first static step, the square plate is subjected to thermal load. Four small transverse forces are applied to the plate corners in this step to induce plate convergence to one of the stable shapes. The forces are removed in the following step to obtain the final equilibrium configuration. The other stable shape can be easily obtained by reversing the direction of the transverse corner forces in the first static step and then following the same modelling procedures.

4.2. Simulation of Snap-Through Process. ABAQUS provides two different methods to solve unstable problems, the "static general" and "static Riks" steps. The former uses the Newton–Raphson method; the latter adopts the modified Riks method to solve nonlinear equilibrium equations [38]. It is well known that the load-displacement response shows a negative stiffness when buckling or collapsing behaviour occurs. Because the Newton method fails in this situation, automatic stabilisation with a damping factor should be applied to achieve convergence [16]. To avoid this problem, the modified Riks method in ABAQUS is used to carry out buckling analysis. Generally, users do not need to take any special precautions in the simulation process.

Following the cooling-down process, transverse concentrated forces are applied to the plate corners in the "static Riks" step. Direction of the point forces is specified contrary to the out-of-plane displacement of the initial stable shape. Because the loading magnitude is part of the solution, we need a method to specify when the step is completed. Here, we specify the maximum displacement value to be the out-of-plane displacement of the other stable shape. The step will terminate once the maximum displacement value is crossed. The whole simulation process in ABAQUS is illustrated in Figure 2.

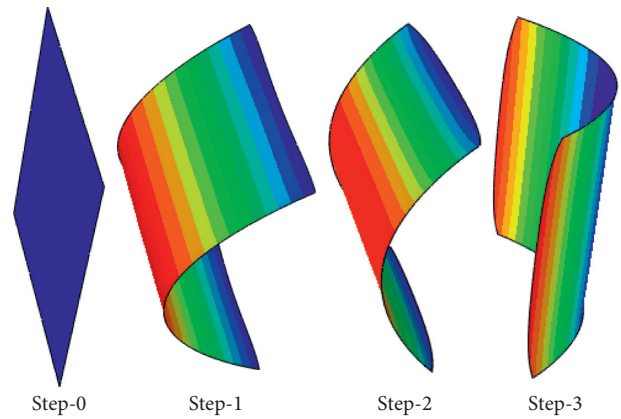

Figure 2: Modelling steps in the FE analysis of the whole simulation process.

Table 1: Material properties of PMMA [31].

ν_h^m	α_h^m (10^{-6}/K)	E_h^m (10^9 Pa)	ρ_h^m (kgm^{-3})
0.34	45 $(1 + 0.0005\Delta T)$	3.51–0.0047 T	1150

5. Results and Discussion

The geometrical configuration displayed in Figure 1 is used to design bistable laminates subjected to thermal load. The $[90/0]_T$ laminate is allowed to cure from high temperature to room temperature, 300 K. Poly(methyl methacrylate), referred to as PMMA, is selected as the matrix of the nanocomposite, and its material parameters are listed in Table 1 [31]. (10, 10) SWCNTs are used as reinforcement in the CNTRC, and its temperature-dependent material properties are predicted by molecular dynamics. Table 2 lists the values for Young's modulus, shear modulus, and thermal expansion coefficient of the SWCNTs under certain temperatures, as given by Shen and Zhang [31]. It should be noted that, to accurately account for the thermal effect, a continuum expression for expansion coefficients is needed in equation (14). This expression can be obtained through curve fitting techniques. Here, a nonlinear function commonly used to describe the temperature-dependent material properties of FG material is used [39]:

$$P_{\text{CN}} = P_0\left(P_{-1}T^{-1} + 1 + P_1T + P_2T^2\right), \quad (31)$$

where P_0, P_{-1}, P_1, and P_2 are the unknown coefficients of temperature T (K) that need to be determined through curve fitting. Using the values in Table 2, the fitting results for the thermal expansion coefficients α_{11}^{CN} and (in 10^{-6}/K) can be calculated; the results are given in Table 3. Because Young's modulus and shear modulus of SWCNTs change little from 300 K to 1000 K, they are assumed to be constant at 300 K. The nanotube volume fractions used in this paper are 0.12, 0.17, and 0.28, unless otherwise stated. The CNT efficiency parameter η_j $(j = 1, 2, 3)$ that corresponds to these volume fractions is given in Table 4 [31].

Table 2: Material properties of (10, 10) SWCNT ($L = 9.26$ nm, $R = 0.68$ nm, $h = 0.067$ nm, $\nu_{12} = 0.175$) [31].

Temperature (K)	E_{11}^{CN} (TPa)	E_{22}^{CN} (TPa)	G_{12}^{CN} (TPa)	α_{11}^{CN} ($\times 10^{-6}$/K)	α_{22}^{CN} ($\times 10^{-6}$/K)
300	5.6466	7.0800	1.9445	3.4584	5.1682
500	5.5308	6.9348	1.9643	4.5361	5.0189
700	5.4744	6.8641	1.9644	4.6677	4.8943
1000	5.2814	6.6220	1.9451	4.2800	4.7532

Table 3: Coefficients for SWCNTs' material properties.

Thermal expansion coefficients	P_0	P_{-1}	P_1	P_2
α_{11}^{CN} (in 10^{-6}/K)	8.107	−146.649	$-2.633e-4$	$-6.213e-8$
α_{22}^{CN} (in 10^{-6}/K)	5.435	0.094	$-1.815e-4$	$5.591e-8$

Table 4: CNT efficiency parameters [31].

Volume fraction	η_1	η_2	η_3
$V_{CN}^* = 0.12$	0.137	1.022	0.715
$V_{CN}^* = 0.17$	0.142	1.626	1.138
$V_{CN}^* = 0.28$	0.141	1.585	1.109

5.1. Temperature Variation. The SWCNTs in this section are assumed to have a linear functionally graded distribution in FG-CNTRC laminates; that is, the volume fraction exponent n equals 1. Most prior mechanical analyses of functionally graded CNTRC plate have followed this assumption [29, 31, 40]. Each layer of the square laminates has a length of 0.3 m and thickness of 0.5 mm. Using the higher-order analytical model described in Section 3.1, we first investigate the effect of curing temperatures on their stable shapes. The out-of-plane displacements for FGX-CNTRC with nanotube volume fraction of 0.28 under curing temperature varying from 301 K to 400 K are calculated and compared with the nonlinear FE analysis. Figure 3 depicts the results of corner out-of-plane displacements versus curing temperatures. The solid lines represent the stable solutions, and the dashed line represents the unstable results. As we can see, for small temperature differences, the plate only has one stable saddle shape. Once the curing temperature exceeds 313 K, bifurcation occurs, and three configurations are obtained: two stable cylindrical shapes and an unstable saddle shape. This phenomenon is very similar to traditional fibre-reinforced bistable composite laminate [32]. The FE analysis displayed in Figure 3 shows the same trend and achieves good agreement with the analytical results.

As mentioned earlier, the analytical model loses accuracy near free edges. Thus, to validate the effectiveness of the higher-order model, the stable cylindrical configurations curing from 400 K to 300 K predicted by the two methods are compared in Figure 4. The discrete dots and the continuum surface correspond to the FE and analytical results, respectively. It can be seen from the error analysis plotted in Figure 5 that the disagreements are mainly observed near the plate edges and their maximum values occur at the four corners. This difference is mainly caused by the approximate displacement polynomial used in the analytical model. Next, we predict the out-of-plane displacements for other types of FG-CNTRC laminates and calculate the relative error at plate corners. According to the results in Table 5, the maximum error is less than 5%. Hence, we can conclude that the higher-order analytical model is accurate in predicting the stable shapes of bistable FG-CNTRC laminates.

The analytical model is then applied to other cases to predict the stable shapes under variable curing temperatures. The FGX- and FGO-CNTRC laminates displayed in Figure 1 with nanotube volume fractions of 0.12, 0.17, and 0.28 are simulated. For quantitative analysis, the geometry and the curing temperatures use the same parameters as the first case. Figure 6 shows the cooling-down bifurcation diagram for six FG-CNTRC laminates. As expected, these plates all possess bistable behaviour after the curing temperatures reach the corresponding values at the bifurcation points; see Table 6. From Figure 6 we can also find that, due to the effect of distribution patterns and nanotube volume fractions, FG-CNTRC plates display different stable shapes for the same curing temperature. For example, the out-of-plane displacements for FG-CNTRC laminates with larger nanotube volume fractions are also greater. This indicates that increasing the nanotube volume fractions is advantageous to the occurrence of bistable behaviour. The reason for this phenomenon is that adding more SWCNTs in nanocomposite leads to increased thermal expansion coefficient mismatch, which in turn induces more residual stresses. Another finding is that changing the distribution types of SWCNTs also influences the stable shapes obtained, but this effect is relatively small.

5.2. Snap-Through Load. A good morphing structure should be easily actuated from one stable shape to another. However, few bistable plates so far developed have achieved this goal, and researchers thus continue to design new kinds of bistable structures [41]. Because adding nanomaterials to polymer can greatly influence its mechanical properties, FG-CNTRC offers the potential for designing bistable plates with

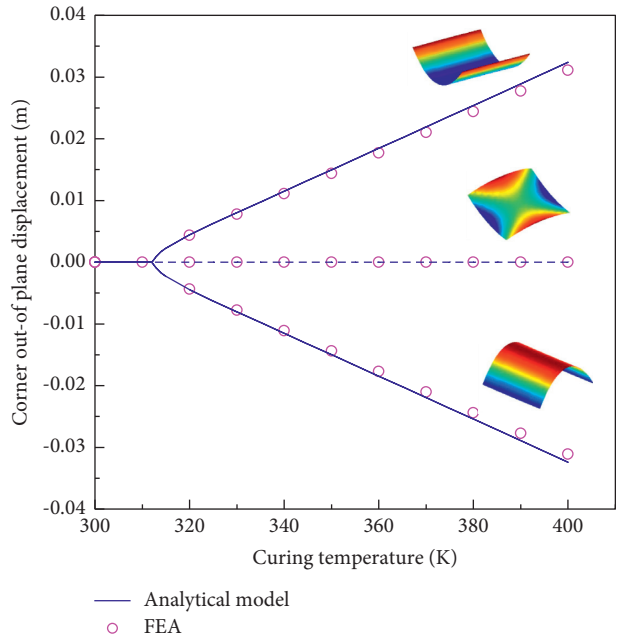

Figure 3: Cooling-down bifurcation diagram: corner out-of-plane displacements against temperature variation (FGX-CNTRC laminate, $V^*_{CN} = 0.28$).

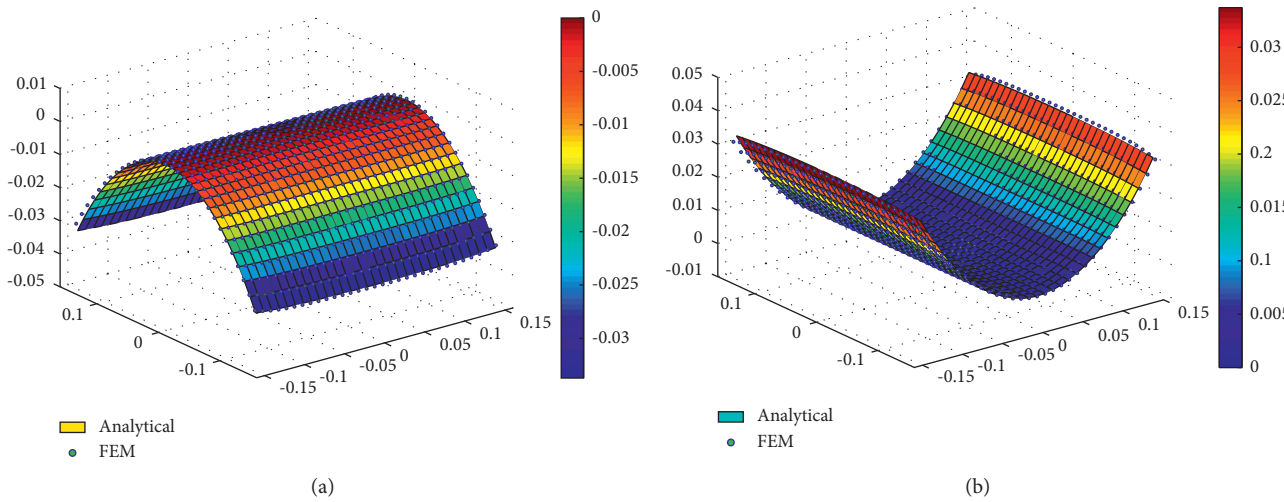

Figure 4: The two stable shapes predicted by the analytical model and the FE analysis ($T_c = 400$ K, FGX-CNTRC laminate, $V^*_{CN} = 0.28$): (a) stable state I; (b) stable state II.

desired stiffness. In this section using the derived analytical model presented in Section 3 and following the simulation steps described in Section 4, the snap-through loads for several cases are predicted.

First, we study the buckling behaviour of FGX-CNTRC laminate with a 0.28 nanotube volume fraction. The simulation starts from one of the stable configurations at room temperature cured from 400 K without applied force. For nonlinear FE analysis, the snap-through process is realised through a buckling analysis using either the "static general" step or "static Riks" step. Figure 7(a) shows the simulated load-displacement diagrams at the plate corner. The geometric configurations at the A, B, C, and D stages are given in Figure 7(b). As can be seen, the Riks and Newton method in ABAQUS both predict the same snap-through force and second stable shape. If "static general" steps are used, in addition to the loading step, an unloading step is also needed to make the plate return to its second stable shape, following the path A-B-E-F-D displayed in Figure 7(a). This is equivalent to the load-controlled test performed in the experiment. With the Riks method, because it can trace the equilibrium path A-B-C-D, only one step is performed in ABAQUS. For this reason, the Riks method has an advantage in predicting the snap-through load. The solid line in Figure 7(a) is our analytical result, which approximates the results of the FE-Riks method well.

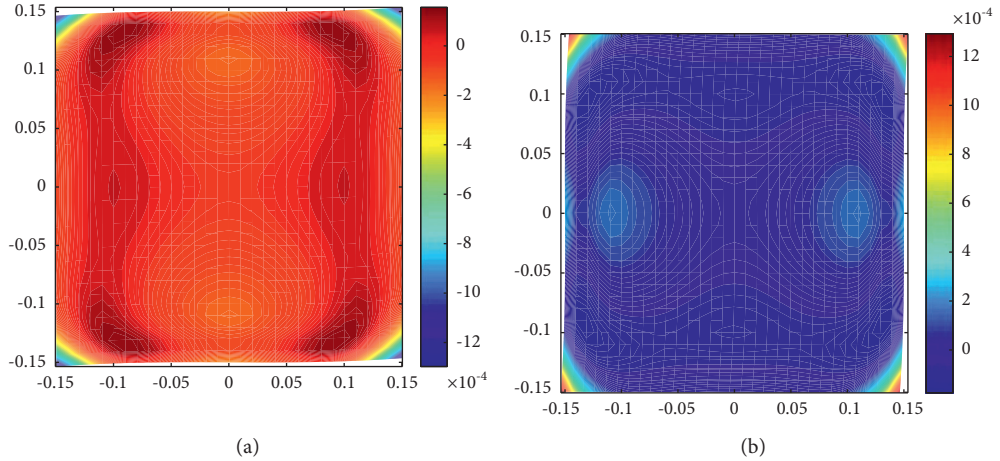

Figure 5: Out-of-plane displacement differences between the analytical model and FEM: (a) stable state I; (b) stable state II.

Table 5: The relative error of corner out-of-plane displacement for bistable FG-CNTRC laminates.

	FGX-CNTRC			FGO-CNTRC		
Volume fractions	0.12	0.17	0.28	0.12	0.17	0.28
FEM	−0.0133	−0.0176	−0.0311	−0.0126	−0.0170	−0.0340
Analytical	−0.0128	−0.0177	−0.0323	−0.0123	−0.0171	−0.0354
Error (%)	3.3	0.2	4.2	2.4	0.5	4.1

Error (%) = |(Analytical − FEM)/FEM|.

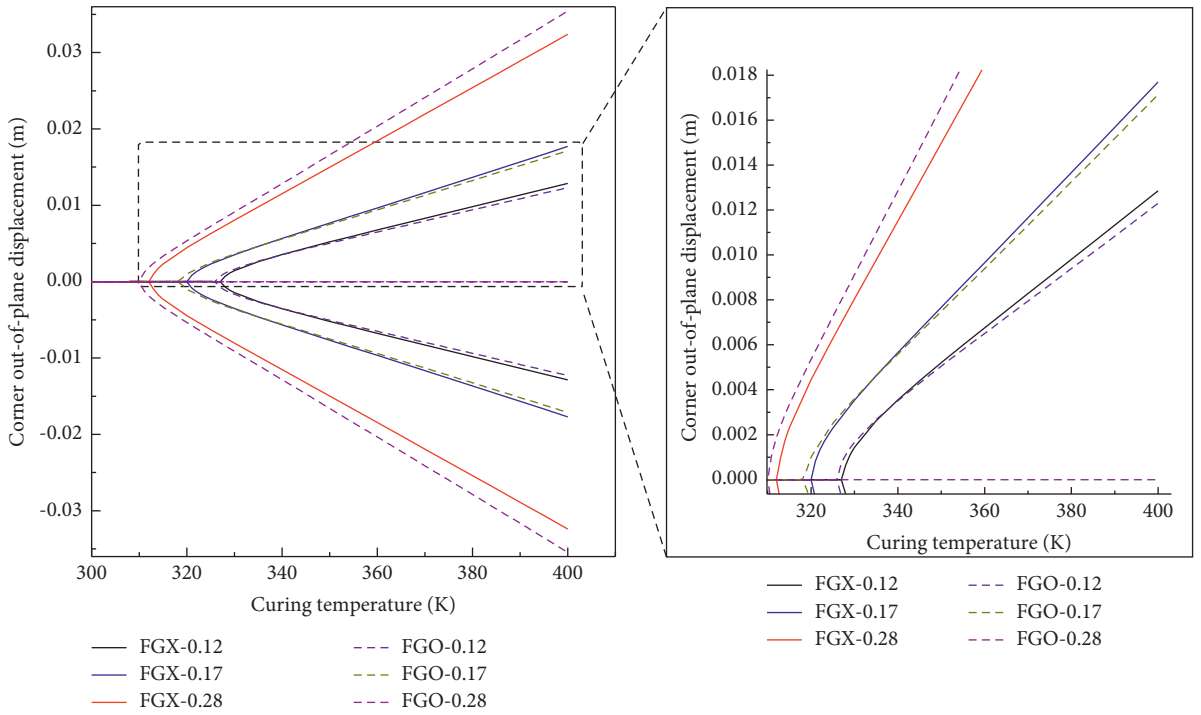

Figure 6: Cooling-down bifurcation diagram: corner out-of-plane displacements against temperature variation (FGX- and FGO-CNTRC laminates, $V_{CN}^{*} = 0.12, 0.17, 0.28$).

Using the "general Riks" step and the higher-order analytical model, we then calculate the snap-through forces for other bistable FG-CNTRC plates. In order to compare their carrying capacity, laminates in these cases are designed to have the same out-of-plane displacement, which is shown in Figure 8. The load-displacement diagrams predicted by the two models are depicted in Figure 9, and Table 7 compares the snap-through forces. From an analysis of

Table 6: Curing temperatures at bifurcation points for FG-CNTRC laminates.

	FGX-CNTRC			FGO-CNTRC		
Volume fractions	0.12	0.17	0.28	0.12	0.17	0.28
Curing temperatures (K)	329	321	313	327	319	311

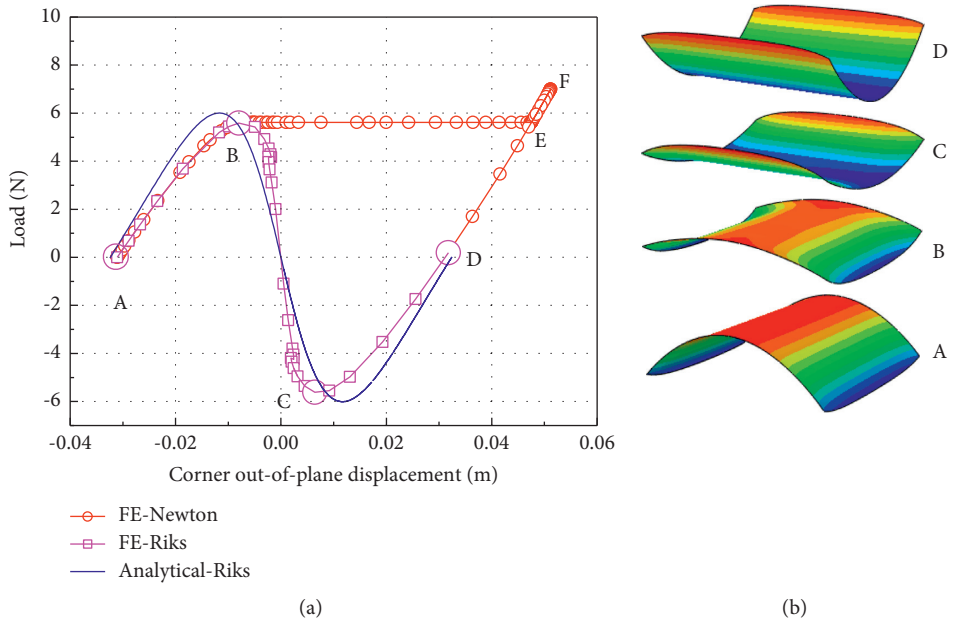

Figure 7: Static snap-through process simulated by FE model. (a) Force-displacement diagrams at the plate corner, (b) corresponding configurations at A, B, C, and D stages in (a).

these data, a trend can be observed: FG-CNTRC laminates with a higher volume fraction of SWCNTs possess greater stiffness. Clearly, adding more SWCNTs can greatly improve the mechanical stiffness of the nanocomposite. In addition, the distribution type of SWCNTs also has a major influence on snap-through forces. It can be seen from Figures 9(g)-9(h) that FGX-CNTRC laminates need larger forces than FGO-CNTRC to induce snap-through. These findings provide a way to design bistable laminates with the desired stiffness by changing the volume fraction and distribution type of reinforcements.

5.3. Variation of Volume Fraction Exponent. From the preceding analysis, we know that changing the distribution type and the volume fraction of SWCNTs in FG-CNTRC laminates is an efficient way to design bistable plates with the desired curvature and stiffness. These cases only consider a linear functionally graded distribution of SWCNTs. To further explore the design space, we assume an exponential distribution of SWCNTs in this section. The distribution of SWCNTs follows a power law that is controlled by the value of exponent n. Figure 10 is a schematic diagram that shows the discrepancy of nanotube distribution in the vicinities of $z=0$ and $z=\pm h$ in the plate when $n=1$, $n<1$, and $n>1$. Obviously, the FG distribution of SWCNTs is closer to a uniform distribution when the exponent has a smaller value. The volume fraction exponents for two layers can have the same or different values, which is discussed in the following parametric studies.

5.3.1. Cross-Ply $[90/0]_T$ FG-CNTRC Plate with the Same Volume Fraction Exponent for Two Layers. We first assume an antisymmetric distribution of SWCNTs in the FG-CNTRC laminates; that is, the nanotube volume fractions and volume fraction exponents for the two layers are each the same. To study the effect of the volume fraction exponent on bistability, curvatures of laminates with volume fraction exponents varying from 0 to 2 are calculated using the higher-order analytical model. Figure 11 shows the relationship between curvature and volume fraction exponents when the curing temperature is 400 K. It can be seen that changing the volume fraction exponent has a similar effect to temperature variation on bistability. When n approaches 0, the cured configuration of FG-CNTRC laminates is a stable saddle shape. By gradually increasing the exponent to a certain value, FG-CNTRC laminates start to possess bistability. The absolute value of the curvature of the two stable cylindrical shapes increases with the rise of n. Hence, a large exponent value is beneficial to the occurrence of bistability. The reason for this phenomenon can be seen in Figure 10, which shows that when the exponent is large, the discrepancy in nanotube distribution in the vicinities of $z=0$ and

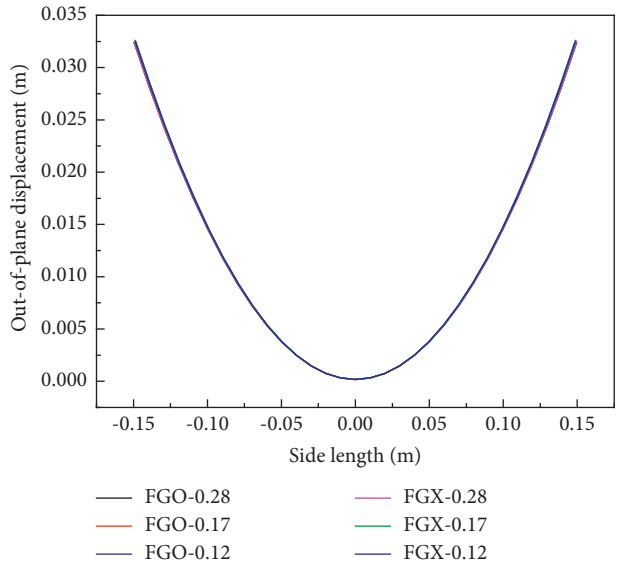

Figure 8: The FG-CNTRC laminates are designed to have the same out-of-plane displacement.

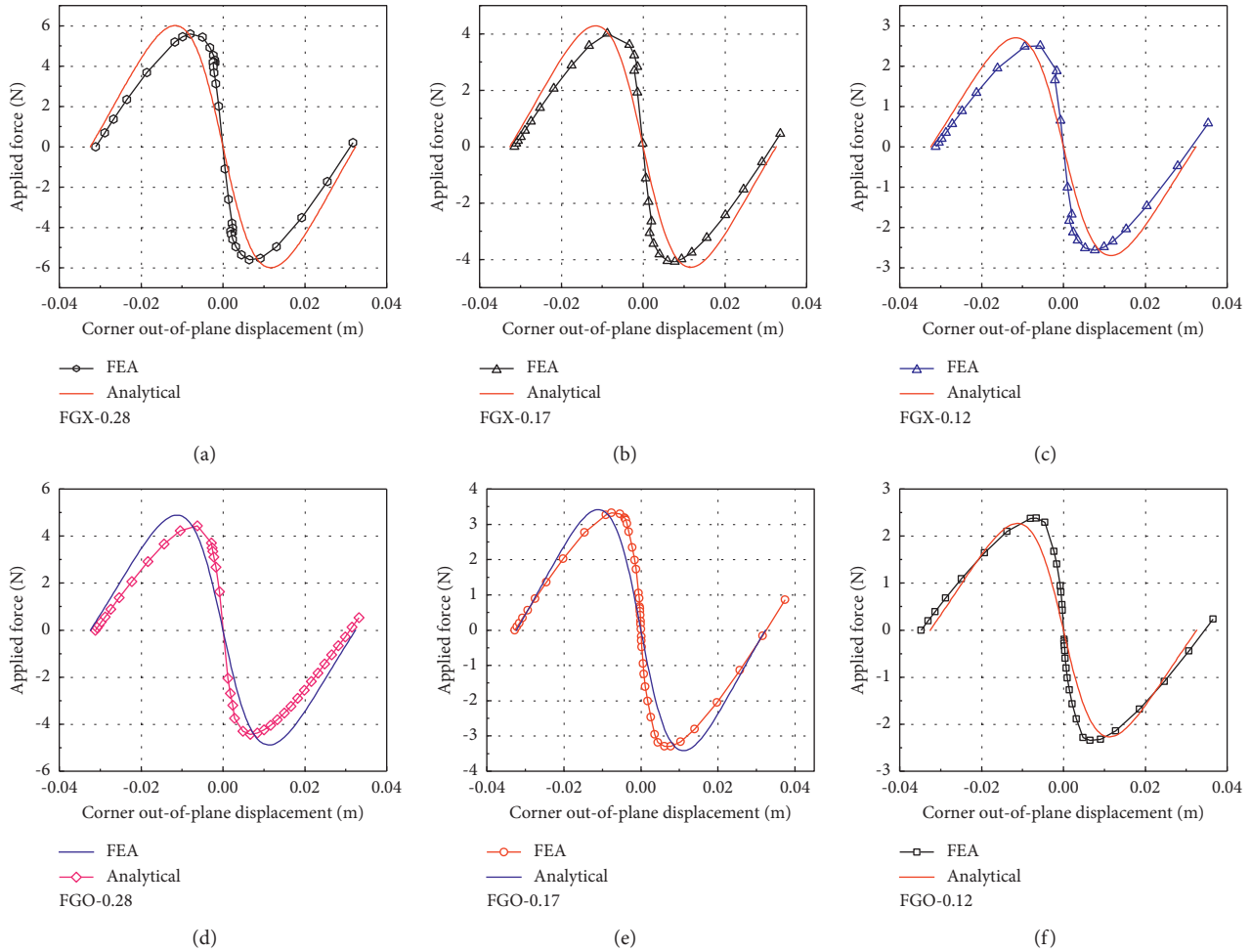

Figure 9: Continued.

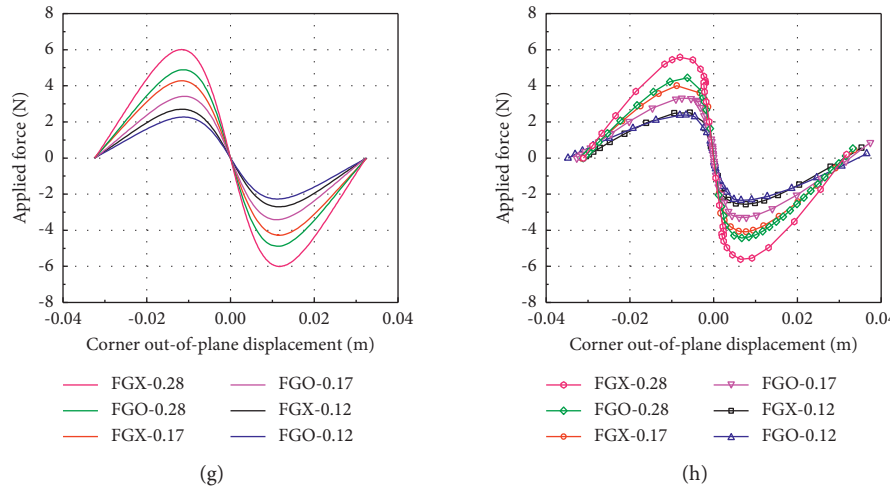

Figure 9: Load-displacement diagrams for bistable FG-CNTRC laminates with the same out-of-plane displacement.

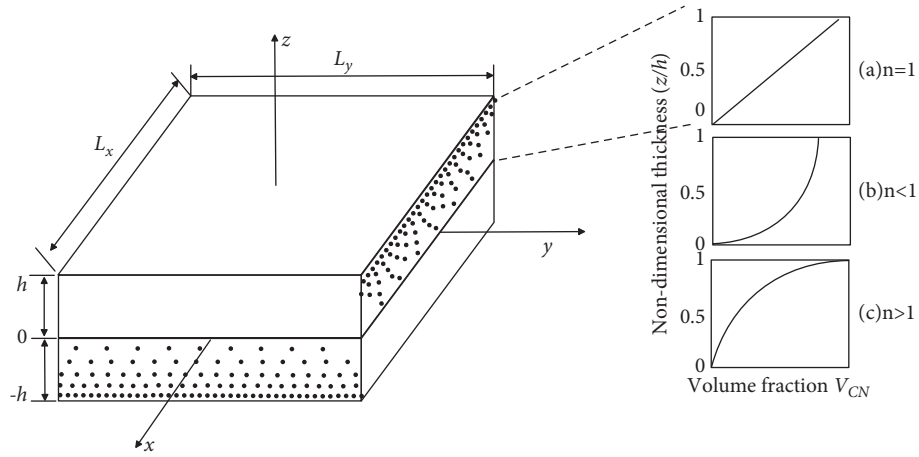

Figure 10: Distribution of SWCNTs in FG-CNTRC plate with the exponents (a) $n = 1$, (b) $n < 1$, and (c) $n > 1$.

Table 7: Comparison of snap-through forces for bistable FG-CNTRC laminates with the same out-of-plane displacement.

	FGX-CNTRC			FGO-CNTRC		
Volume fractions	0.12	0.17	0.28	0.12	0.17	0.28
Curing temperature	525	473	400	535	478	392
Snap-through force (N)						
FEM	2.50	4.00	5.59	2.38	3.32	4.44
Analytical	2.70	4.28	6.00	2.27	3.41	4.89
Error (%)	8	7	7.3	4.6	2.7	10.1

Error (%) = |(Analytical − FEM)/FEM|.

$z = \pm h$ is also large. Because the anisotropy of thermal properties of SWCNTs is small, this discrepancy largely accounts for the degree of mismatch in thermal expansion coefficients between two layers and the thermal residual stresses.

Four values (0.5, 1, 1.5, and 2) are then selected for the volume fraction exponent n to calculate the snap-through forces for these plates, so that the effect of the volume fraction exponent on their stiffness can be studied. Again, these plates are allowed to have the same cylindrical shape. The simulation results for snap-through forces and curing temperatures are listed in Table 8. Analysis of these data reveals that, for FG-CNTRC laminate with the same volume fraction of SWCNTs, decreasing the volume fraction exponent will improve stiffness. Hence, we conclude that uniformly distributed SWCNTs in nanocomposites can increase their stiffness but are disadvantageous for inducing bistability.

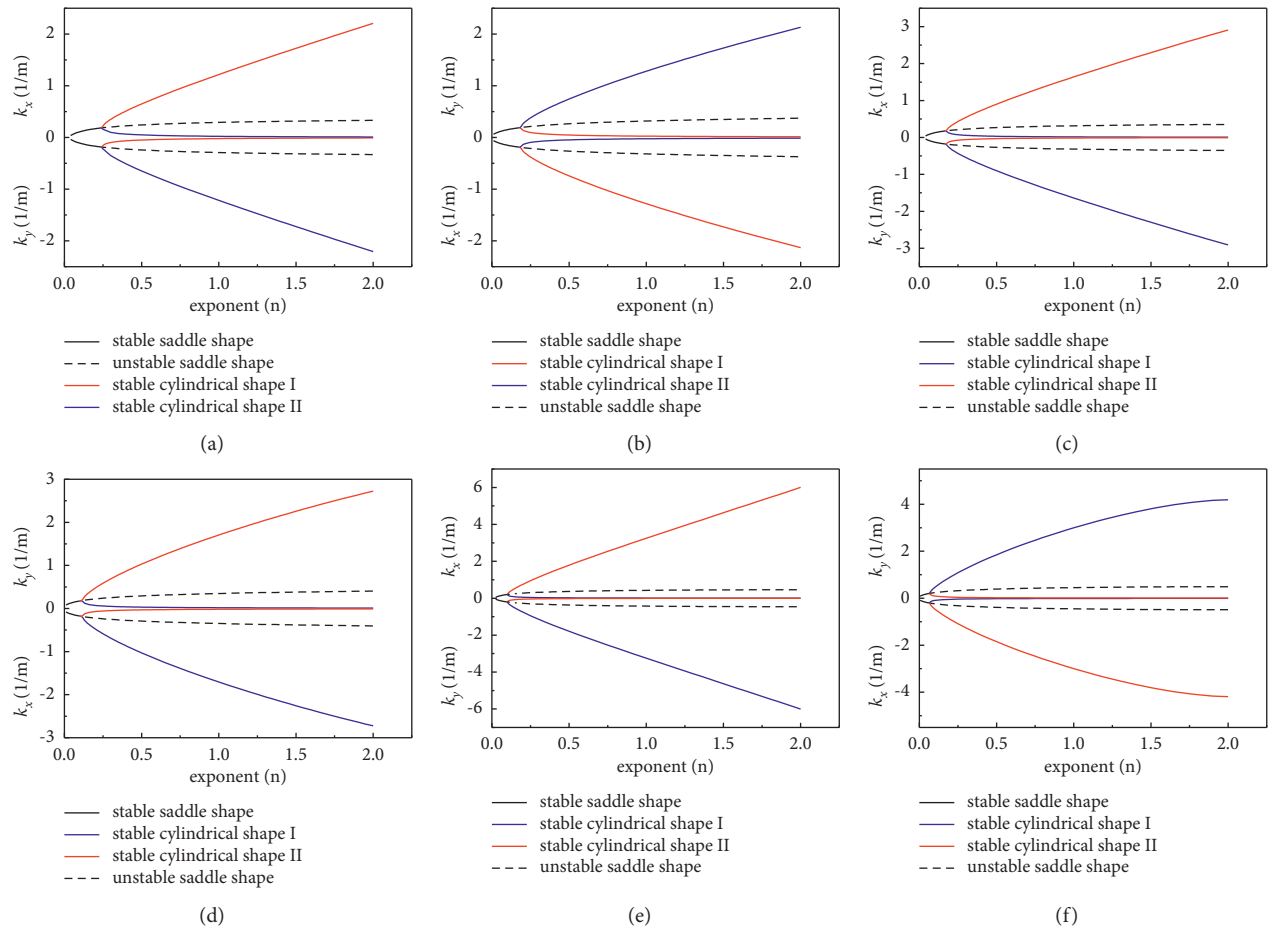

Figure 11: Exponent-curvature relations for FG-CNTRC laminates ($T_c = 400$ K): (a) FGO-CNTRC laminate, $V^*_{CN} = 0.12$; (b) FGX-CNTRC laminate, $V^*_{CN} = 0.12$; (c) FGO-CNTRC laminate, $V^*_{CN} = 0.17$; (d) FGX-CNTRC laminate, $V^*_{CN} = 0.17$; (e) FGO-CNTRC laminate, $V^*_{CN} = 0.28$; (f) FGX-CNTRC laminate, $V^*_{CN} = 0.28$.

Table 8: Snap-through forces for bistable FG-CNTRC laminates with different volume fraction exponents, n.

		FGX-CNTRC			FGO-CNTRC		
		0.12	0.17	0.28	0.12	0.17	0.28
Snap-through force (N)	$n = 0.5$	1.099	1.718	2.397	1.011	1.556	2.175
	$n = 1$	1.043	1.653	2.331	0.882	1.362	1.930
	$n = 1.5$	1.026	1.617	2.308	0.801	1.221	1.723
	$n = 2$	0.984	1.596	2.282	0.731	1.096	1.584
Curing temperature (K)	$n = 0.5$	515	462	393	539	481	395
	$n = 1$	431	400	358	436	403	353
	$n = 1.5$	399	376	345	398	374	337
	$n = 2$	380	363	341	377	358	328

5.3.2. Cross-Ply $[90/0]_T$ FG-CNTRC Plate with Different Volume Fraction Exponents for Two Layers. Cross-ply FG-CNTRC laminate with different volume fraction exponents for the two layers can be viewed as bonding together two layers of lamina with different material properties. This stacking sequence makes it possible to design bistable laminates with two different stable cylindrical shapes. Figure 12 displays four cases of FG-CNTRC laminates in which the distribution of SWCNTs follows a linear function and a power law for the lower and upper layer, respectively. n_0 and n_{90} represent the value of the volume fraction exponent for the lower and upper layer. By keeping the value of n_0 unchanged and varying n_{90} from 0.1 to 2, we predict the stable shapes of FG-CNTRC laminates cured from 400 K to 300 K. Taking FGO-CNTRC laminate with 0.28 nanotube volume fraction as an example, Figure 13(a) depicts the relationship

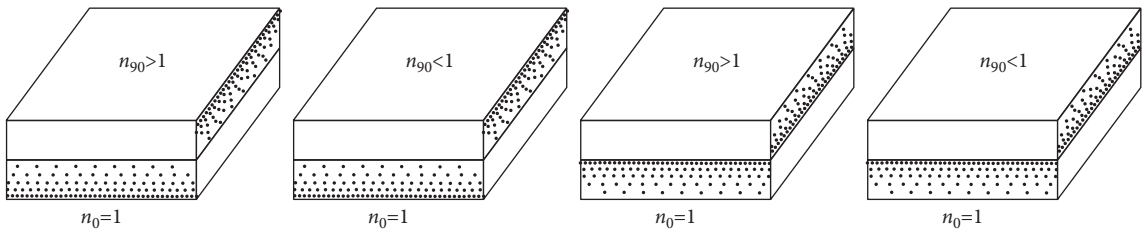

FIGURE 12: $[90/0]_T$ FG-CNTRC laminates with different volume fraction exponents: (a) and (b) are FGX-CNTRC laminates; (c) and (d) are FGO-CNTRC laminates.

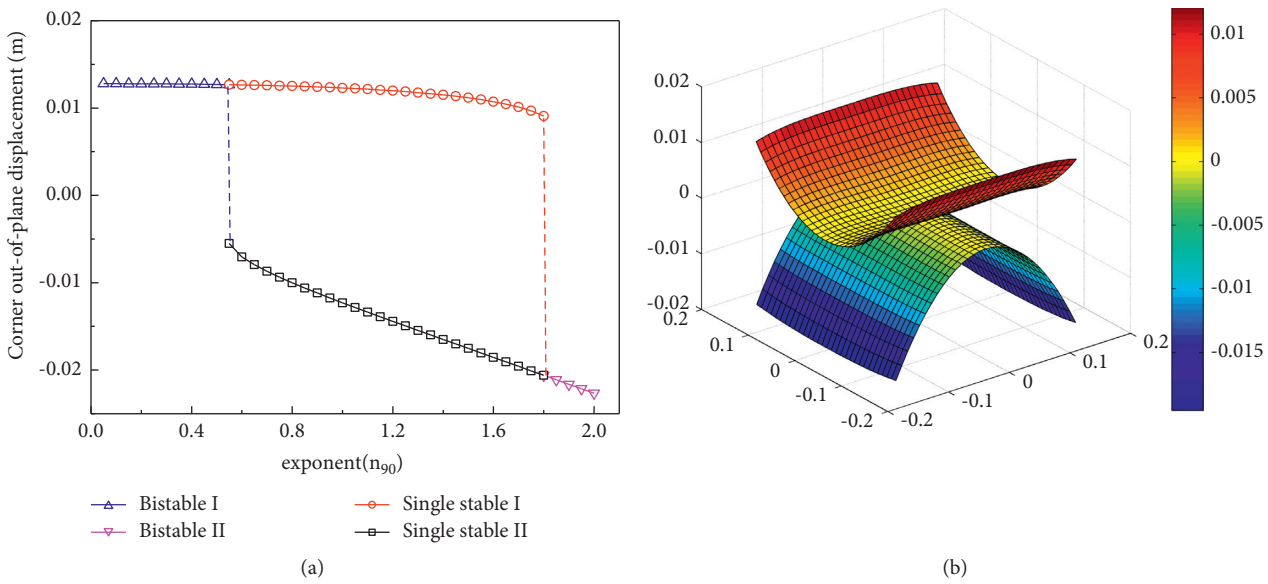

FIGURE 13: Thermally induced bistable laminates with two different cylindrical shapes: (a) corner out-of-plane displacement vs. volume fraction exponent; (b) two stable shapes when $n_0 = 1$, $n_{90} = 1.6$; FGO-CNTRC, $V^*_{CN} = 0.12$.

between the corner out-of-plane displacements and n_{90}. It can be seen that when the difference between n_0 and n_{90} is large ($n_{90} > 1.8$ and $n_{90} < 0.55$), the laminates are predicted to have a single stable cylindrical shape. When n_{90} changes from 0.55 to 1.8, two stable cylindrical shapes are observed, and if n_0 is not equal to n_{90}, the out-of-plane displacements for the two stable shapes are different; one example of this is illustrated in Figure 13(b). The physics behind this phenomenon are explained by the degree of mismatch in the thermal residual stress in the x and y directions.

To investigate the carrying capacity, snap-through loads for bistable laminates with different stable cylindrical shapes are determined using nonlinear FE analysis and the higher-order analytical model. Figure 14(a) depicts the load-displacement diagrams simulated by FE, and Figure 14(b) presents the simulation results of the analytical model. The snap-through loads simulated by two methods are listed in Table 9. As we can see, the two methods predict very similar paths and snap-through loads. Because there are two different cylindrical shapes for bistable laminates, the loads needed to induce snap-through and snap-back are also different. The load-displacement diagrams show that the values of the snap-through forces for stable shapes with larger out-of-plane displacements are also higher. Note that Figure 14 only presents the load-displacement diagrams of laminates with bistability. For laminates with a single stable shape, their snap-through loads can be interpreted as the buckling loads of a cylindrical shell.

Finally, the bistability of other cases of FG-CNTRC laminates with varying volume fraction exponents are studied using the higher-order analytical model. The values of n_{90} are allowed to vary from 0.6 to 1.8 at 0.2 intervals. The predicted corner out-of-plane displacements and the snap-through forces are summarised in Table 10. For FGX-CNTRC laminates without bistability, we only list the corner out-of-plane displacements and the buckling loads for the single stable cylindrical shape. These data provide rich information on bistable plates generated using FG-CNTRC laminates, which have a wide range of out-of-plane displacements and carrying capacities. It is hence advantageous to use FG-CNTRC laminates to design bistable plates rather than traditional fibre-reinforced composite laminates.

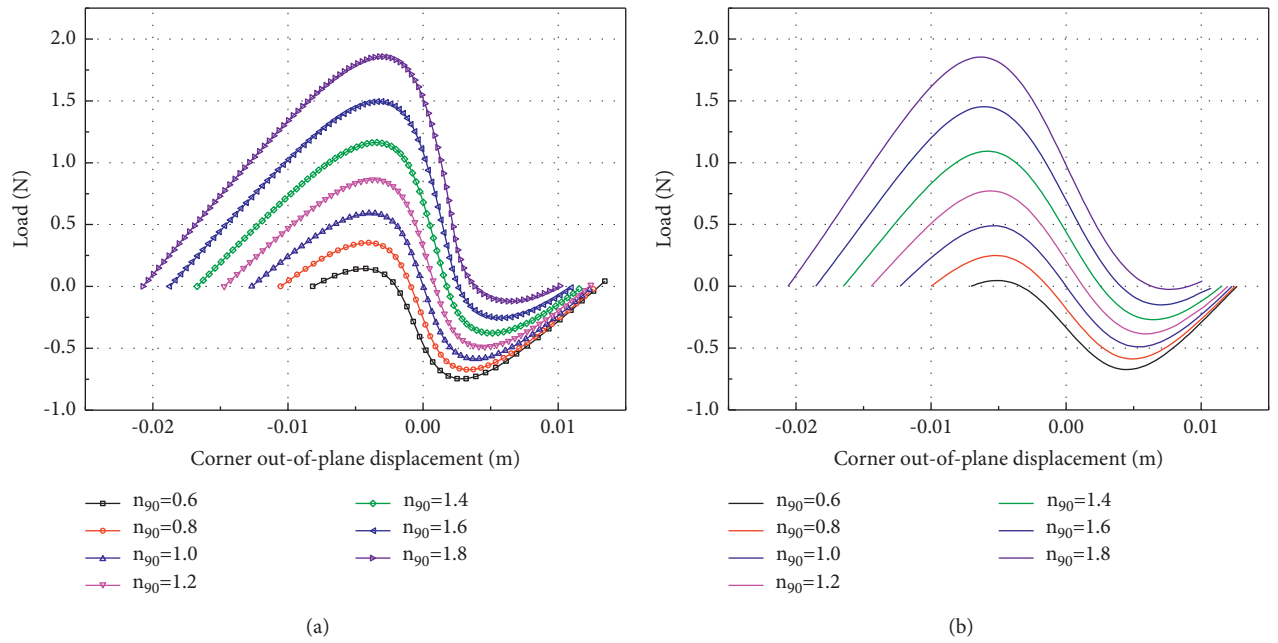

Figure 14: Load-displacement diagrams of $[90/0]_T$ FGO-CNTRC laminates with different volume fraction exponents for two layers: (a) ABAQUS; (b) analytical ($n_0 = 1$, $V^*_{CN} = 0.12$).

Table 9: Comparison of snap-through forces for bistable FG-CNTRC laminates with different volume fraction exponents for two layers.

	Volume fraction exponent		Snap-through force (N) FEM		Snap-through force (N) analytical	
	n_0	n_{90}	Stable I	Stable II	Stable I	Stable II
FGO-CNTRC	1	0.6	0.145	−0.745	0.049	−0.673
		0.8	0.353	−0.673	0.249	−0.587
		1.0	0.592	−0.586	0.489	−0.489
		1.2	0.861	−0.488	0.771	−0.384
		1.4	1.162	−0.376	1.092	−0.270
		1.6	1.494	−0.255	1.452	−0.150
		1.8	1.858	−0.120	1.853	−0.025

Table 10: Corner out-of-plane displacements and snap-through forces of FG-CNTRC laminates with different volume fraction exponents of SWCNTs (upper layer). "—" means that a stable shape does not exist for this case.

FG-CNTRC	Volume fraction exponent		Corner out-of-plane displacement (m)		Snap-through force (N)	
	n_0	n_{90}	Stable I	Stable II	Stable I	Stable II
FGO-0.28	1	0.6	−0.02609	0.03556	2.254	−6.345
		0.8	−0.03079	0.03550	3.787	−5.974
		1.0	−0.03544	0.03544	5.570	−5.571
		1.2	−0.04011	0.03540	7.611	−5.153
		1.4	−0.04483	0.03538	9.894	−4.689
		1.6	−0.04961	0.03543	12.430	−4.234
		1.8	−0.05443	0.03558	15.217	−3.748
FGO-0.17	1	0.6	−0.01120	0.01726	0.307	−1.612
		0.8	−0.01433	0.01722	0.756	−1.461
		1.0	−0.01714	0.01714	1.292	−1.292
		1.2	−0.01986	0.01699	1.918	−1.106
		1.4	−0.02258	0.01677	2.629	−0.907
		1.6	−0.02532	0.01645	3.430	−0.701
		1.8	−0.02810	0.01595	4.315	−0.487

Table 10: Continued.

FG-CNTRC	Volume fraction exponent		Corner out-of-plane displacement (m)		Snap-through force (N)	
	n_0	n_{90}	Stable I	Stable II	Stable I	Stable II
FGX-0.28	1	0.6	−0.03631	0.01919	8.276	−1.051
		0.8	−0.03451	0.02633	7.214	−3.373
		1.0	−0.03238	0.03238	6.002	−6.003
		1.2	−0.02983	0.03812	4.629	−8.925
		1.4	−0.02661	0.04373	3.068	−12.141
		1.6	−0.02199	0.04926	1.267	−15.658
		1.8	—	0.05476	—	−19.499
FGX-0.17	1	0.6	−0.01995	—	2.615	—
		0.8	−0.01892	0.01360	2.155	−0.715
		1.0	−0.01770	0.01770	1.653	−1.652
		1.2	−0.01619	0.02131	1.113	−2.698
		1.4	−0.01408	0.02474	0.541	−3.842
		1.6	—	0.02808	—	−5.085
		1.8	—	0.03139	—	−6.422
FGX-0.12	1	0.6	−0.01450	—	1.048	—
		0.8	−0.01376	0.00959	0.841	−0.219
		1.0	−0.01286	0.01286	0.617	−0.616
		1.2	−0.01166	0.01559	0.378	−1.059
		1.4	−0.00979	0.01812	0.129	−1.546
		1.6	—	0.02057	—	−2.078
		1.8	—	0.02296	—	−2.652

6. Conclusions

In this paper, we consider the advantages of thermally induced bistable plates made of functionally graded carbon nanotube-reinforced composite (FG-CNTRC). In the $[90/0]_T$ laminates, single-walled carbon nanotubes (SWCNTs) are assumed to have a functionally graded distribution across the thickness direction following an exponential function. A higher-order analytical model is developed to investigate the cooling-down process and buckling behaviours of the proposed bistable FG-CNTRC laminates. The simulation results are compared using nonlinear finite element analysis and achieve good agreement. Through the parametric study, some interesting findings are obtained:

(1) Adding more SWCNTs in nanocomposite can enlarge the mismatch of thermal expansion coefficients between two layers of cross-ply FG-CNTRC laminates, which is beneficial for the occurrence of bistability.

(2) A bistable FG-CNTRC plate with larger nanotube volume fraction possesses higher stiffness, and thus it is more stable with bearing larger loading. And FGX-CNTRC plates are stiffer than FGO-CNTRC plates.

(3) Changing the volume fraction exponent of SWCNTs can influence the stable shapes and snap-through forces of bistable FG-CNTRC plates. Thus, a large volume fraction exponent is beneficial to the occurrence of bistability but is disadvantageous to increasing the plate stiffness.

(4) Bonding together two layers of FG-CNTRC lamina with different volume fraction exponents of SWCNTs can obtain bistable plates with two different stable shapes. These plates are predicted to have a wide range of out-of-plane displacements and carrying capacities, indicating great potential for applications in morphing structures in the future.

In summary, the residual thermal stresses that accumulate during the cooling-down process and the plate stiffness can be easily adjusted by varying the distribution type, volume fraction, and volume fraction exponent of SWCNTs. This study has proved that FG-CNTRC laminate is a good candidate for bistable plate design.

Data Availability

The data have been included within the article.

Conflicts of Interest

The authors declare that they have no conflicts of interest.

Acknowledgments

This work is supported by the National Natural Science Foundation of China under Grant no. 41877251 and China Postdoctoral Science Foundation funded project under Grant no. 2021M691427.

References

[1] M. W. Hyer, "Some observations on the cured shape of thin unsymmetric laminates," *Journal of Composite Materials*, vol. 15, no. 2, pp. 175–194, 1981.

[2] M. W. Hyer and P. C. Bhavani, "Suppression of anticlastic curvature in isotropic and composite plates," *International*

Journal of Solids and Structures, vol. 20, no. 6, pp. 553–570, 1984.

[3] M. L. Dano and M. W. Hyer, "Thermally-induced deformation behavior of unsymmetric laminates," *International Journal of Solids and Structures*, vol. 35, no. 17, pp. 2101–2120, 1998.

[4] M. L. Dano and M. W. Hyer, "Snap-through of unsymmetric fiber-reinforced composite laminates," *International Journal of Solids and Structures*, vol. 39, no. 1, pp. 175–198, 2002.

[5] S. A. Emam, "Snapthrough and free vibration of bistable composite laminates using a simplified Rayleigh-Ritz model," *Composite Structures*, vol. 206, pp. 403–414, 2018.

[6] Z. Wu, H. Li, and M. I. Friswell, "Advanced nonlinear dynamic modelling of bi-stable composite plates," *Composite Structures*, vol. 201, pp. 582–596, 2018.

[7] Z. Zhang, H. Wu, X. He, H. Wu, Y. Bao, and G. Chai, "The bistable behaviors of carbon-fiber/epoxy anti-symmetric composite shells," *Composites Part B: Engineering*, vol. 47, pp. 190–199, 2013.

[8] O. Bilgen, A. F. Arrieta, M. I. Friswell, and P. Hagedorn, "Dynamic control of a bistable wing under aerodynamic loading," *Smart Materials and Structures*, vol. 22, no. 2, Article ID 25020, 2013.

[9] X. Lachenal, S. Daynes, and P. M. Weaver, "Review of morphing concepts and materials for wind turbine blade applications," *Wind Energy*, vol. 16, no. 2, pp. 283–307, 2013.

[10] S. Daynes and P. M. Weaver, "Review of shape-morphing automobile structures: concepts and outlook," *Proceedings of the Institution of Mechanical Engineers - Part D: Journal of Automobile Engineering*, vol. 227, no. 11, pp. 1603–1622, 2013.

[11] A. F. Arrieta, P. Hagedorn, A. Erturk, and D. J. Inman, "A piezoelectric bistable plate for nonlinear broadband energy harvesting," *Applied Physics Letters*, vol. 97, no. 10, Article ID 104102, 2010.

[12] A. F. Arrieta, T. Delpero, A. E. Bergamini, and P. Ermanni, "Broadband vibration energy harvesting based on cantilevered piezoelectric bi-stable composites," *Applied Physics Letters*, vol. 102, no. 17, Article ID 173904, 2013.

[13] W. Hufenbach, M. Gude, L. Kroll, A. Sokolowski, and B. Werdermann, "Adjustment of residual stresses in unsymmetric fiber-reinforced composites using genetic algorithms," *Mechanics of Composite Materials*, vol. 37, no. 1, pp. 71–78, 2001.

[14] W. Hufenbach, M. Gude, and L. Kroll, "Design of multistable composites for application in adaptive structures," *Composites Science and Technology*, vol. 62, no. 16, pp. 2201–2207, 2002.

[15] M. Gigliotti, M. R. Wisnom, and K. D. Potter, "Loss of bifurcation and multiple shapes of thin [0/90] unsymmetric composite plates subject to thermal stress," *Composites Science and Technology*, vol. 64, no. 1, pp. 109–128, 2004.

[16] C. G. Diaconu, P. M. Weaver, and A. F. Arrieta, "Dynamic analysis of bi-stable composite plates," *Journal of Sound and Vibration*, vol. 322, no. 4-5, pp. 987–1004, 2009.

[17] Z. Zhang, H. Wu, G. Ye, J. Yang, S. Kitipornchai, and G. Chai, "Experimental study on bistable behaviour of anti-symmetric laminated cylindrical shells in thermal environments," *Composite Structures*, vol. 144, pp. 24–32, 2016.

[18] S. Daynes, K. Potter, and P. Weaver, "Bistable prestressed buckled laminates," *Composites Science and Technology*, vol. 68, no. 15-16, pp. 3431–3437, 2008.

[19] H. Li, F. Dai, P. M. Weaver, and S. Du, "Bistable hybrid symmetric laminates," *Composite Structures*, vol. 116, pp. 782–792, 2014.

[20] X. Q. He, L. Li, S. Kitipornchai, C. M. Wang, and H. P. Zhu, "Bi-stable Analyses of laminated fgm shells," *International Journal of Structural Stability and Dynamics*, vol. 12, no. 2, pp. 311–335, 2012.

[21] Z. Zhang, B. Chen, C. Lu et al., "A novel thermo-mechanical anti-icing/de-icing system using bi-stable laminate composite structures with superhydrophobic surface," *Composite Structures*, vol. 180, pp. 933–943, 2017.

[22] F. Mattioni, P. M. Weaver, and M. I. Friswell, "Multistable composite plates with piecewise variation of lay-up in the planform," *International Journal of Solids and Structures*, vol. 46, no. 1, pp. 151–164, 2009.

[23] C. S. Sousa, P. P. Camanho, and A. Suleman, "Analysis of multistable variable stiffness composite plates," *Composite Structures*, vol. 98, pp. 34–46, 2013.

[24] A. F. Arrieta, I. K. Kuder, T. Waeber, and P. Ermanni, "Variable stiffness characteristics of embeddable multi-stable composites," *Composites Science and Technology*, vol. 97, pp. 12–18, 2014.

[25] I. K. Kuder, A. F. Arrieta, and P. Ermanni, "Design space of embeddable variable stiffness bi-stable elements for morphing applications," *Composite Structures*, vol. 122, pp. 445–455, 2015.

[26] A. Haldar, J. Reinoso, E. Jansen, and R. Rolfes, "Thermally induced multistable configurations of variable stiffness composite plates: semi-analytical and finite element investigation," *Composite Structures*, vol. 183, pp. 161–175, 2018.

[27] H. S. Shen, "Nonlinear bending of functionally graded carbon nanotube-reinforced composite plates in thermal environments," *Composite Structures*, vol. 91, no. 1, pp. 9–19, 2009.

[28] M. Rafiee, J. Yang, and S. Kitipornchai, "Large amplitude vibration of carbon nanotube reinforced functionally graded composite beams with piezoelectric layers," *Composite Structures*, vol. 96, pp. 716–725, 2013.

[29] M. Rafiee, X. Q. He, and K. M. Liew, "Nonlinear analysis of piezoelectric nanocomposite energy harvesting plates," *Smart Materials and Structures*, vol. 23, no. 6, Article ID 65001, 2014.

[30] K. M. Liew, Z. X. Lei, and L. W. Zhang, "Mechanical analysis of functionally graded carbon nanotube reinforced composites: a review," *Composite Structures*, vol. 120, pp. 90–97, 2015.

[31] H. S. Shen and C. L. Zhang, "Thermal buckling and post-buckling behavior of functionally graded carbon nanotube-reinforced composite plates," *Materials & Design*, vol. 31, no. 7, pp. 3403–3411, 2010.

[32] A. Pirrera, D. Avitabile, and P. M. Weaver, "Bistable plates for morphing structures: a refined analytical approach with high-order polynomials," *International Journal of Solids and Structures*, vol. 47, no. 25-26, pp. 3412–3425, 2010.

[33] J. N. Reddy, *Mechanics of Laminated Composite Plates and Shells: Theory and Analysis*, CRC Press, Boca Raton, F L, USA, 2004.

[34] E. Riks, "An incremental approach to the solution of snapping and buckling problems," *International Journal of Solids and Structures*, vol. 15, no. 7, pp. 529–551, 1979.

[35] M. A. Crisfield, "A fast incremental/iterative solution procedure that handles "snap-through"," *Computational Methods in Nonlinear Structural and Solid Mechanics*, vol. 13, pp. 55–62, 1981.

[36] B. A. Memon and X. Z. Su, "Arc-length technique for nonlinear finite element analysis," *Journal of Zhejiang University - Science*, vol. 5, no. 5, pp. 618–628, 2004.

[37] S. Tawfik, X. Tan, S. Ozbay, and E. Armanios, "Anticlastic stability modeling for cross-ply composites," *Journal of Composite Materials*, vol. 41, no. 11, pp. 1325–1338, 2006.
[38] M. Smith, *ABAQUS/Standard User's Manual, Version 6.9*, Dassault Systémes Simulia Corp, Providence, RI, USA, 2009.
[39] X. Q. He, T. Y. Ng, S. Sivashanker, and K. M. Liew, "Active control of FGM plates with integrated piezoelectric sensors and actuators," *International Journal of Solids and Structures*, vol. 38, no. 9, pp. 1641–1655, 2001.
[40] M. Rafiee, X. Q. He, and K. M. Liew, "Non-linear dynamic stability of piezoelectric functionally graded carbon nanotube-reinforced composite plates with initial geometric imperfection," *International Journal of Non-linear Mechanics*, vol. 59, pp. 37–51, 2014.
[41] A. J. Lee, A. Moosavian, and D. J. Inman, "Control and characterization of a bistable laminate generated with piezoelectricity," *Smart Materials and Structures*, vol. 26, no. 8, Article ID 85007, 2017.